J Fail. Anal. and Preven.
DOI 10.1007/s11668-017-0291-6

TECHNICAL ARTICLE—PEER-REVIEWED

Potentiodynamic Polarization Behavior and Pitting Corrosion Analysis of 2101 Duplex and 301 Austenitic Stainless Steel in Sulfuric Acid Concentrations

Roland Tolulope Loto · Cleophas Akintoye Loto

Submitted: 16 March 2017 / in revised form: 10 May 2017

Abstract The corrosion behavior of 2101 duplex and 301 austenitic stainless steel in the presence of sulfate (SO_4^{2-}) anion concentrations was investigated through polarization techniques, weight loss and optical microscopy analysis. The corrosion rates of the steels were comparable after 3M H_2SO_4. Results confirm that the duplex steel displayed a higher resistance to pitting corrosion than the austenitic steel. Experimental observation shows that its pitting potential depends on the concentration of the SO_4^{2-} ions in the acid solution due to adsorption of anions at the metal-film interface. The duplex steel underwent stable pitting at relatively higher potentials and significantly higher corrosion current than the austenitic steel. The duplex steel exhibited lower corrosion potential values thus less likely to polarize in the acid solution. Solution concentration had a limited influence on the polarization behavior of the austenitic steel and hence its reaction to SO_4^{2-} ion penetration from analysis of the pitting potentials and observation of its narrower polarization scans compared to the duplex steel which showed wide scatter over the potential domain with changes in concentration.

Keywords Pitting · Corrosion · Steel · Acid · Polarization

R. T. Loto · C. A. Loto
Department of Mechanical Engineering, Covenant University, Ota, Ogun State, Nigeria

R. T. Loto (✉) · C. A. Loto
Department of Chemical Metallurgical and Materials Engineering, Tshwane University of Technology, Pretoria, South Africa
e-mail: tolu.loto@gmail.com

Introduction

Stainless steels have wide-spread applications industrially due to their resistance to corrosion resulting from the formation of a passive protective film. This film is due to the presence of chromium and other important alloying elements. It tends to destabilize in the presence of aggressive sulfate anions, especially in sites or regions of inclusions, impurities, grain boundaries and other flaws which lead to localized corrosion [1]. The major source of corrosive sulfates is sulfuric acid, which is the most important and widely used industrial chemical worldwide. Its corrosivity on stainless steel alloys varies depending on the concentration and type of alloy. Most of the sulfuric acid encountered is in diluted concentrations for many chemical processes, ore refining, petroleum production and water treatment. This tends to result in the initiation and growth of pitting corrosion. Pitting is a localized corrosion attack that occurs at small discrete areas due to the action of aggressive anions, such as chlorides [2]. Criteria such as pitting potential, passivation potential and anodic potential have been used to define and assess pitting corrosion through known electrochemical techniques [3]. With respect to considerable successes in research, more still needs to be done to understand the phenomenon due to the differential nature of alloy chemistry, defects in passive films and the presence of impurities and inclusions. Numerous studies performed on metastable and stable pit growth have seen considerable progress on propagation processes, conditions and effects of electrochemical variables [4–7]. Several mechanisms have been proposed to explain the passivity breakdown [8]. However, the mechanisms of the pit initiation related to passivity breakdown in sulfate solutions is rare, especially the penetration of sulfate anions through the passive films.

Published online: 26 June 2017

Experimental Methods

Materials and Preparation

2101 duplex and 310 austenitic stainless steels sourced commercially had a nominal composition as shown in Table 1. The steel specimens after machining were abraded with silicon carbide papers (80, 320, 600, 800 and 1000 grits) before washing with distilled water and propanone, and kept in a desiccator for coupon analysis and potentiodynamic polarization tests according to ASTM G1 - 03(2011) [9].

Potentiodynamic Polarization Technique

Polarization measurements were taken at 30°C using a three-electrode system and glass cell containing 200 mL of the corrosive test solution with Digi-Ivy 2311 electrochemical workstation. 2101SS and 301SS electrodes mounted in acrylic resin with an exposed surface area of 2.54 and 0.72 cm^2 were prepared according to ASTM G59-97(2014) [10]. Polarization plots were obtained at a scan rate of 0.0015 V/s between potentials of −0.5 and +1.5 V according to ASTM G102-89(2015) [11]. A platinum rod was used as the counter electrode and a silver chloride electrode (Ag/AgCl) as the reference electrode. Corrosion current density (j_{cr}) and corrosion potential (E_{cr}) values were obtained using the Tafel extrapolation method. The corrosion rate (γ) and the inhibition efficiency (η_2, %) were calculated from the mathematical relationship;

$$C_R = \frac{0.00327 \times J_{corr} \times E_{qv}}{D} \quad \text{(Eq 1)}$$

j_{corr} is the current density in A/cm^2, D is the density in g/cm^3, E_{qv} is the sample equivalent weight in grams, and 0.00327 is a constant for corrosion rate calculation in mm/year [12].

Weight Loss Measurement

Measured 2101SS and 301SS coupons with exposed surface areas of 9.61 and 3.82 cm^2 were separately immersed in 200 mL of the dilute acid test solution for 240 h at 30°C and weighed every 24 h according to ASTM NACE/ASTMG31-12a [13]. Corrosion rate (C_R) is determined as follows as [14];

$$C_R = \left[\frac{87.6\omega}{DAT}\right] \quad \text{(Eq 2)}$$

ω is the weight loss in g, D is the density in g/cm^3, A is the total surface area of the coupon in cm^2, and 87.6 is a constant.

Optical Microscopy Characterization

Images of control and corroded 2101SS and 301SS surface morphologies from optical microscopy were analyzed after weight loss measurement with an Omax trinocular metallurgical through the aid of ToupCam analytical software.

Result and Discussion

Potentiodynamic Polarization Studies

The corrosion polarization behavior of 2101SS and 301SS specimens in 1–6M H_2SO_4 acid media is shown in Figs. 1 and 2. Tables 2 and 3 present the data for the potentiodynamic polarization plots. 2101SS specimens displayed slightly lower corrosion rate values than 301SS at 1–3M H_2SO_4 acid concentration. The variation in corrosion rate for the two steel specimens increased from 4M to 6M H_2SO_4 solution concentration with a corresponding higher increase in corrosion current. 2101SS exhibited more positive corrosion potential values than 301SS at all H_2SO_4 concentrations studied. The corrosion potential of 2101SS peaked at 3M H_2SO_4 and decrease slightly till 6M H_2SO_4. This confirms the corrosion rate results as 301SS with a lower (more negative) corrosion potential is more likely to

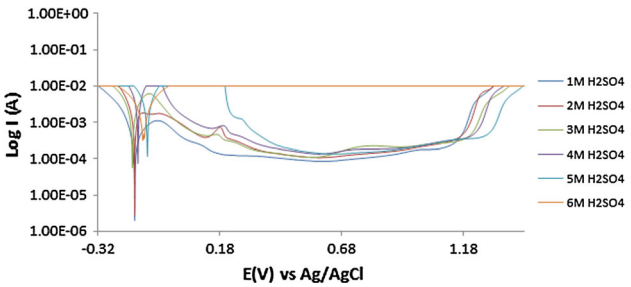

Fig. 1 Potentiodynamic polarization curves of 2101SS in 1–6M H_2SO_4 solutions

Table 1 Percentage nominal composition of 2101SS and 301SS

Element symbol	Mo	Si	Ni	Cr	Mn	P	N	C	Fe
% Composition (2101SS)	0.4	1	1.8	22.8	4	0.04	0.2	0.03	69.7
% Composition (301SS)	0	1	8	16	2	0.045	0.1	0.15	72.7

polarize in the acid solution. The anodic-cathodic polarization scans for 301SS (Fig. 4) were quite similar after 1M H_2SO_4 when compared to 2101SS (Fig. 3) which showed wide scatter over the potential domain. This shows that changes in solution concentration have limited influence on the polarization behavior of 301SS and hence its reaction to the SO_4^{2-} ion penetration of its passive film. At 1–2M H_2SO_4, the peak anodic-cathodic current (E_{corr}) of 2101SS is minimal at 2.69 × 10 A/−168 $mV_{Ag/AgCl}$. An increase in SO_4^{2-} ion concentration over 2M H_2SO_4 caused a sharp and progressive increase in the anodic-cathodic peak current (E_{corr}) until 6M H_2SO_4 (4.05 × 10^{-4} A, peak current). A close view of sample F plot (Fig. 3) at 6M H_2SO_4 showed multiple anodic-cathodic peak current signifying unstable passivation before anodic polarization. The lowest anodic-cathodic peak current for 301SS is 1.29 × 10^{-6} A at 6M H_2SO_4, while its highest value is 3.93 × 10^{-5} A at 4M H_2SO_4.

The austenite/ferrite metallurgical structure of the 2101SS coupled with its higher chromium content enhanced its corrosion resistance when compared to 301SS with an austenite microstructure stabilized by its higher nickel content than 2101SS and lower chromium content. The alloy surface of 301SS tends to more easily form soft acid, from the concept Lewis acid-base theory, thus adsorbing sulfate ions and molecules resulting in covalent bonds between the steel and the adsorbates which accelerates its corrosion rate faster than the 2101SS [15]. This is responsible for the breakdown of the passive film in the presence of aggressive sulfates ions which causes localized

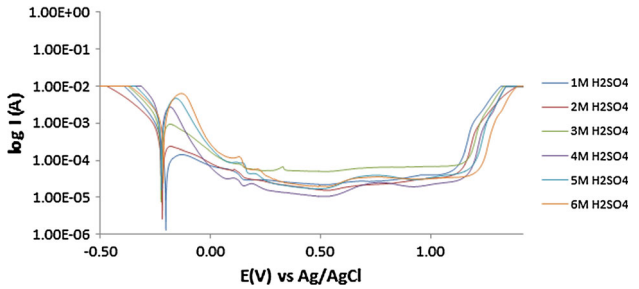

Fig. 2 Potentiodynamic polarization curves of 3101SS in 1–6M H_2SO_4 solutions

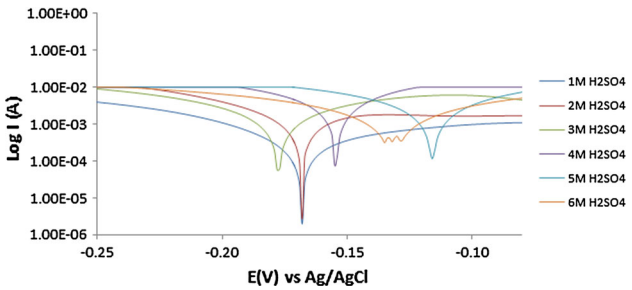

Fig. 3 Current peaks of 2101SS in 1–6M H_2SO_4 solution

Table 2 Polarization results for 2101SS in 1–6M H_2SO_4

Sample	Acid conc. (M)	Corrosion rate (mm/year)	Corrosion current (A)	Corrosion current density (A/cm^2)	Corrosion potential (V)	Polarization resistance (R_p)	Cathodic Tafel slope (B_c)	Anodic Tafel slope (B_a)
A	1	2.19	5.17E–04	2.04E–04	−0.168	−299.61	−7.855	−0.143
B	2	1.28	3.02E–04	1.19E–04	−0.168	−430.11	−6.866	−0.120
C	3	12.90	3.05E–03	1.20E–03	−0.178	−40.29	−4.671	−0.114
D	4	21.42	5.06E–03	1.99E–03	−0.154	−23.62	−3.261	−0.112
E	5	26.08	6.16E–03	2.42E–03	−0.116	−18.03	−4.592	−0.103
F	6	31.67	7.48E–03	2.94E–03	−0.132	−13.62	−5.153	−0.094

Table 3 Polarization results for 301SS in 1–6M H_2SO_4

Sample	Acid conc. (M)	Corrosion rate (mm/year)	Corrosion current (A)	Corrosion current density (A/cm^2)	Corrosion potential (V)	Polarization resistance (R_p)	Cathodic Tafel slope (B_c)	Anodic Tafel slope (B_a)
A	1	2.62	1.51E–04	2.51E–04	−0.202	185.15	−0.044	0.031
B	2	6.03	3.47E–04	5.79E–04	−0.218	77.47	−8.804	0.102
C	3	18.97	1.09E–03	1.82E–03	−0.224	26.41	−8.156	0.109
D	4	31.00	1.78E–03	2.97E–03	−0.224	14.74	−8.636	0.100
E	5	37.54	2.16E–03	3.60E–03	−0.222	13.57	−7.705	0.111
F	6	44.49	2.56E–03	4.27E–03	−0.214	7.33	−4.891	0.071

corrosion of the underlying metal. The higher corrosion current exhibited by 2101SS at lower corrosion potentials suggests that the passive film thickness of the steel is much higher than that of 301SS; thus, it takes a longer time to locally dissolve and thin out before the underlying metal begins to corrode [16–18]. The explanations hold for 2101SS specimens A-D; specimen E showed delayed passivation behavior until -170 $mV_{Ag/AgCl}$ in the acid solution due to the strong adsorption of excess anions at 5M H_2SO_4, while specimen F showed weak passivation at 6M H_2SO_4 as earlier mentioned; however, their corrosion rates are comparatively better than those of 301SS at the same H_2SO_4 concentrations.

Pitting Corrosion Evaluation

2101SS specimens underwent stable pitting at relatively higher potentials (pitting potential, E_{pitt}) and significantly higher corrosion current than 301SS at a scan rate of 0.0015 V/s versus Ag/AgCl (Tables 4 and 5). Resistance to pit formation is responsible for the higher corrosion density of 2101SS at E_{pitt} following the metastable pitting activity in the passivity region of potentiodynamic tests. The increase in anodic current density with increasing electrode potential signifies the onset of transpassivation of the steel specimens [19, 20]. 301SS showed generally uniform but narrower passivation behavior over the potentiostatic domain at the solution concentrations and retained its passivation behavior at 6M H_2SO_4 in comparison with 2101SS which showed unstable passivation at the acid concentration. Experimental observation shows that E_{pitt} depends on the concentration of the SO_4^{2-} ions in the acid solution. Beyond the transpassive region of the potentiostatic domain of both steel specimens, Cr(III) oxide is oxidized to Cr(VI) oxide coupled with the loss of the protective film [21, 22].

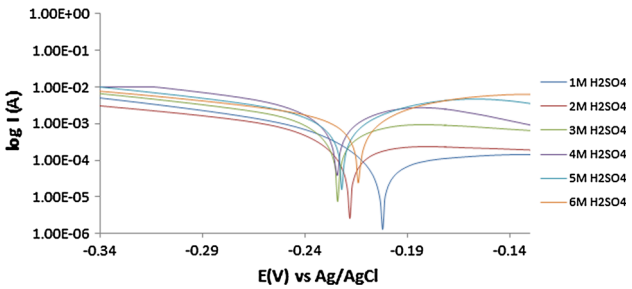

Fig. 4 Current peaks of 301SS in 1–6M H_2SO_4 solution

The occurrence of metastable pits on the polarization plots of 2101SS and 301SS was quite similar. Increase in solution concentration caused a significant rise in passivation current density for both steels which eventually led to a progressive increase in the metastable region of the polarization plots, an indication that the passive film is undergoing localized but transient pitting due to temporary breakdown of the passive film, and the creation and growth of small, occluded cavities before stable passivation. These events are determined by the steel composition and the quality of the passive film. Comparison of the passivation potential in Tables 5 and 6 shows that 2101SS passivated at higher potentials and higher passivation current densities

Table 4 Potentiostatic data of pitting and passivation potentials for 2101SS in 1–6M H_2SO_4 solution

Sample	Acid concentration (M)	Pitting potential (V) (E_{pitt})	Current at E_{pitt} (A)	Passivation potential (V)	Current at passivation potential (V)
A	1	1.09	1.88E–04	−0.11	8.81E–04
B	2	1.17	2.94E–04	−0.11	1.65E–03
C	3	1.15	2.97E–04	−0.13	4.83E–03
D	4	1.16	3.34E–04	−0.11	9.94E–03
E	5	1.25	3.79E–04	−0.15	9.94E–03
F	6	0	0	0	0

Table 5 Potentiostatic data of pitting and passivation potentials for 301SS in 1–6M H_2SO_4 solution

Sample	Acid concentration (M)	Pitting potential (V) (E_{pitt})	Current at E_{pitt} (A)	Passivation potential (V)	Current at passivation potential (V)
A	1	1.05	4.17E–05	−0.18	1.05E–04
B	2	1.10	3.92E–05	−0.23	2.04E–04
C	3	1.10	7.25E–05	−0.20	7.07E–04
D	4	1.11	2.73E–05	−0.20	2.16E–03
E	5	1.13	4.41E–05	−0.18	3.46E–03
F	6	1.16	3.67E–05	−0.17	4.62E–03

Table 6 Results of weight loss measurement for 2101SS in 1–6M H_2SO_4 at 240 h

Sample	Acid concentration (M)	Weight loss (g)	Corrosion rate (mm/year)
A	1	0.002	0.000006
B	2	0.070	0.000274
C	3	3.054	0.011909
D	4	5.137	0.020032
E	5	7.874	0.030705
F	6	9.149	0.035677

Table 7 Results of weight loss measurement for 301SS in 1–6M H_2SO_4 at 240 h

Samples	Acid concentration (M)	Weight loss (g)	Corrosion rate (mm/year)
A	1	0.0015	0.00003
B	2	1.0112	0.01810
C	3	1.3141	0.02352
D	4	1.3914	0.02490
E	5	1.9582	0.03504
F	6	1.9957	0.03571

following anodic polarization with a minimum value of -110 $mV_{Ag/AgCl}$ and maximum at -150 $mV_{Ag/AgCl}$ compared to the values for 301SS at -170 $mV_{Ag/AgCl}$ and -230 $mV_{Ag/AgCl}$. 301SS showed a consistent increase in passivation current density with increase in SO_4^{2-} ion concentration, showing the direct relationship between both parameters. Increase in passivation current density for 2101SS stalled after specimen D at 4M H_2SO_4.

Loss of passivity responsible for pitting corrosion in steel alloys is due to a variety of different proposed mechanisms. The three main mechanisms are (a) penetration mechanism, (b) film breaking mechanism and (c) adsorption mechanism [23, 24]. Observing the proportional increase in passivation and pitting current densities with increase in acid concentration for 2101SS, it is assumed that adsorption of aggressive SO_4^{2-} ions at the metal-film interface at varying concentrations induces the electrolytic transport of metallic cations to the acid solution. The resulting formation of complexes and formation of corrosion pits through SO_4^{2-} ions which has been known to delay the formation of pits in chloride containing environments [25]. This causes the accelerated weakening of the protective film and start of the anodic metal dissolution at higher corrosion potentials. As earlier mentioned, the presence of Cr(III) oxide being oxidized to Cr(VI) oxide is due possibly to the displacement of the oxygen atom, which chemically combines with chromium in the acid solution. Adsorption of the SO_4^{2-} ions onto the protective

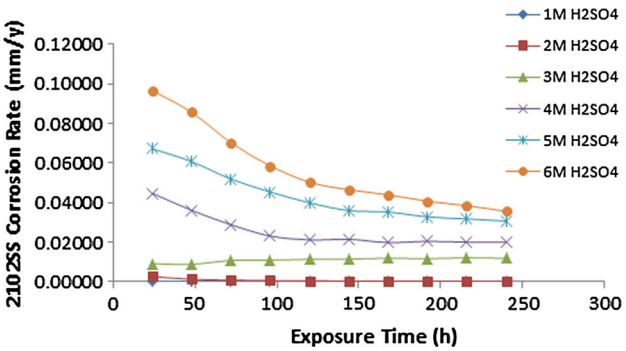

Fig. 5 Plot of corrosion rate vs. exposure time for 2101SS in 1–6M H_2SO_4

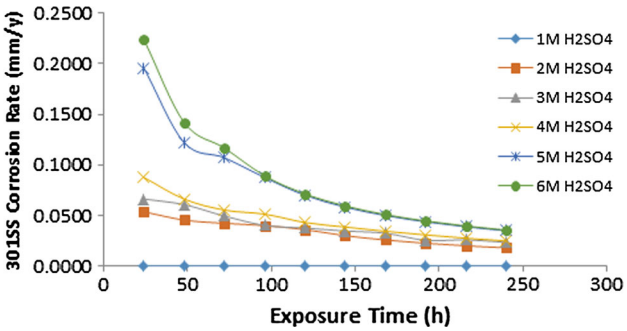

Fig. 6 Plot of corrosion rate vs. exposure time for 301SS in 1–6M H_2SO_4

film surface limits the amount of oxygen vacancies, causing increase in metallic cation transport into the solution. The redox mechanism accelerates the transfer of metallic cations into the acid solution leading to the creation of more metallic vacancies at the metal/film interface, which eventually forms voids and pit initiation [22, 26].

Studying the marginal increase in pitting corrosion potential of 301SS with respect to its current density at pitting, it can be observed that SO_4^{2-} ion concentration has limited influence on the pitting corrosion characteristics of the steel. Penetration of the aggressive anions through the protective film to the metal/film interface through sites of inclusions, cracks and breakage of the passive film is suggested by which the anions diffuse through the oxide film to the metal surface and breakdown of the film occurring when they reach the substrate metal. The film was undermined by the resulting cationic and oxygen vacancies leading to weakening of the passive film and dissolution of the steel alloy [27–32].

Weight Loss Measurements and Optical Microscopy Analysis

Corrosion rate results from weight loss measurement for 301SS and 2101SS specimens are shown in Tables 6

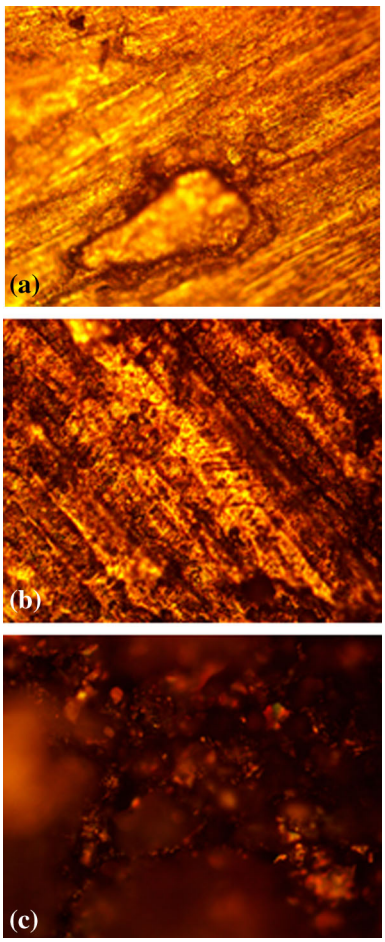

Fig. 7 Optical microscopy images of 2101SS at mag ×40 (**a**) control specimen, (**b**) 1M H_2SO_4 and (**c**) 5M H_2SO_4

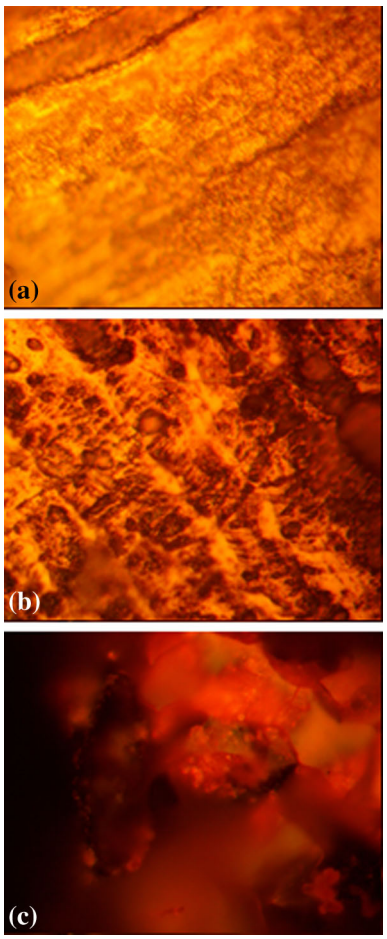

Fig. 8 Optical microscopy images of 2101SS at mag ×100 (**a**) control specimen, (**b**) 1M H_2SO_4 and (**c**) 5M H_2SO_4

and 7. The graphical illustration of corrosion rates versus exposure hours in the acid solution is shown in Figs. 5 and 6. Figures 7 and 8 show the micrographs of 2101SS before corrosion, after 1M acid corrosion and after 5M acid corrosion, while Figs. 9 and 10 show the micrographs of 301SS, respectively, at magnification ×40 and ×100. Susceptibility to pitting and general corrosion is given by the weight loss due to dissolution of chromium-depleted areas of the specimens. The steel specimens corroded at generally the same rates in the acid media after 2M H_2SO_4 with 2101SS exhibiting a slightly higher corrosion resistance. At 1M H_2SO_4, the corrosion rate of both steels is significantly different (0.000006 and 0.00003 mm/year), after which there was a large increase in the corrosion rate of 301SS. The micrographs of the corroded samples at this concentration show a slightly significant contrast between the control and corroded specimens (Figs. 7a, b, 8a, b, 9a, b, and 10a, b). The morphology of 2101 at this concentration shows a surface deteriorating generally over the metal substrate and the presence of macro-pits. 310SS specimens show deterioration occurring more at the grain boundaries signifying intergranular corrosion as the onset of the surface deterioration. The corrosion rate of 2101SS remained significantly low at 2M H_2SO_4 after which it significantly increased till 6M H_2SO_4. Observing the corrosion behavior of the steels on the graphical plot (Figs. 5 and 6), 2101SS at 3–6M H_2SO_4 was susceptible to accelerated corrosion from the onset of the exposure period before stabilizing at 150 h. This phenomenon of accelerated corrosion was observed for 301SS at slightly higher corrosion rate values for the same acid concentration; however, its corrosion rates progressively decreased to the end of the exposure period. Depletion in the chromium oxide and iron content of metallic alloys due to initial precipitation of the chromium rich phases is responsible for their corrosion susceptibility. The above observation shows that 301SS experiences a higher degree of metallic dissolution compared to 2101SS [33].

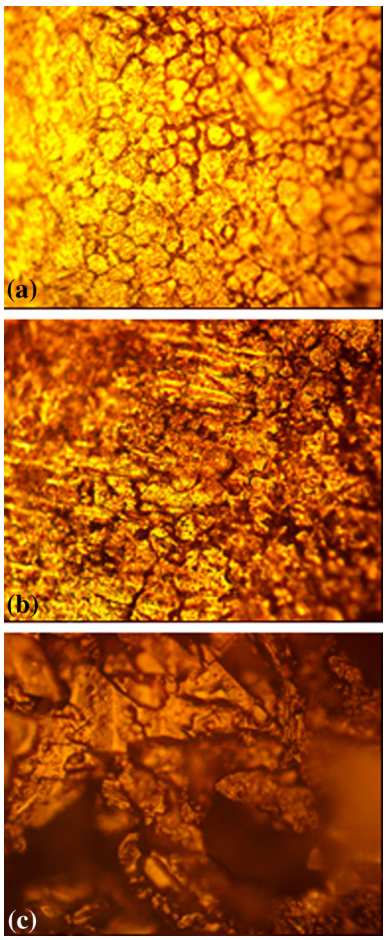

Fig. 9 Optical microscopy images of 3101SS at mag ×40 (**a**) control specimen, (**b**) 1M H_2SO_4 and (**c**) 5M H_2SO4

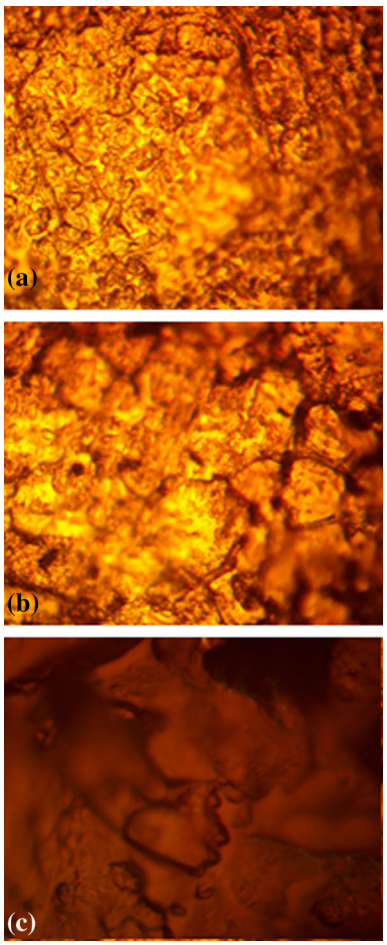

Fig. 10 Optical microscopy images of 301SS at mag ×100 (**a**) control specimen, (**b**) 1M H_2SO_4 and (**c**) 5M H_2SO_4

An increase in SO_4^{2-} ion concentration resulted in a significant decrease in the strength of the passive film as the metal electro-dissolution reaction dominated the corrosion reaction mechanism at solution concentrations above 2M. This confirms that the SO_4^{2-} ions penetrate through the passive films of the stainless steels and upon reaching the metal/film interface results in film breakdown as earlier discussed. This is confirmed from the micrographs in Figs. 5c, 6c, 7c, and 8c. It is observed in the figures that 310SS morphology is covered with black oxides (ferrous ferric oxide) with micro-pits. 2101SS exhibited general surface deterioration with numerous micro-pits. Both steel specimens demonstrated the same passivation behavior from the plot with respect to solution concentration. The corrosion resistance of 2101SS is due to the presence of chromium oxides within the protective film as a result of its higher chromium content when compared to 301SS. It is believed that the chromium content caused the formation of wider insoluble Cr_2O_3, which slowed down the deterioration of the alloy [34–37].

Conclusion

2101 duplex stainless steel showed significantly higher corrosion resistance compared to 301 austenitic stainless steel at 1–2M H_2SO_4 after which the difference was narrow till 6M H_2SO_4. Pitting corrosion resistance studies showed the duplex steel to be more resistant due to its austenite/ferrite metallurgical structure, coupled with its higher chromium content which enhances its corrosion resistance in comparison to 301 austenitic steel with its austenite microstructure stabilized by its higher nickel content than the duplex steel and lower chromium content. The duplex steel underwent stable pitting at relatively higher potentials and significantly higher corrosion current than the austenitic steel. SO_4^{2-} ion concentration had limited influence on the pitting corrosion characteristics of 301 austenitic steel. Penetration of the aggressive anions through the protective film occurred presumably through inclusions, cracks and breakage of the film. The proportional increase in passivation and pitting current densities with increase in

acid concentration for 2101 duplex steel shows that adsorption of aggressive SO_4^{2-} ions at the metal-film interface at varying concentrations induces the electrolytic transport of metallic cations to the acid solution, resulting in the formation of complexes and formation of corrosion pits. Comparison of the passivation potential shows that the duplex steel passivated at higher potentials and higher passivation current densities following anodic polarization.

References

1. D.E. Williams, M.R. Kilburn, J. Cliff, G.I.N. Waterhouse, Composition changes around sulphide inclusions in stainless steels, and implications for the initiation of pitting corrosion. Corros. Sci. **52**, 3702–3716 (2010)
2. D.A. Jones, *Principles and Prevention of Corrosion* (Macmillan Publishing Company, New York, 1992), p. 208
3. R.W. Revie, H.H. Uhlig, *Corrosion and Corrosion Control* (Wiley, New Jersey, 2008)
4. P.C. Pistorius, G.T. Burstein, Metastable pitting corrosion of stainless steel and the transition to stability. Philos. Trans.: Phys. Sci. Eng. **341**, 531–559 (1992)
5. P.C. Pistorius, G.T. Burstein, Growth of corrosion pits on stainless steel in chloride solution containing dilute sulphate. Corros. Sci. **33**, 1885–1897 (1992)
6. P. Ernst, N.J. Laycock, M.H. Moayed, R.C. Newman, The mechanism of lacy cover formation in pitting. Corros. Sci. **39**, 1133–1136 (1997)
7. N.J. Laycock, R.C. Newman, Temperature dependence of pitting potentials for austenitic stainless steels above their critical pitting temperature. Corros. Sci. **40**, 887–902 (1998)
8. J. Soltis, Passivity breakdown, pit initiation and propagation of pits in metallic materials—review. Corros. Sci. **90**, 5–22 (2015)
9. ASTM G1 - 03(2011) Standard Practice for Preparing, Cleaning, and Evaluating Corrosion Test Specimens. http://www.astm.org/Standards/G1. Retrieved 30 May 2016
10. ASTM G59 - 97(2014) Standard Test Method for Conducting Potentiodynamic Polarization Resistance Measurements. http://www.astm.org/Standards/G31 Retrieved 30 May 2016
11. ASTM G102 - 89(2015)e1 Standard Practice for Calculation of Corrosion Rates and Related Information from Electrochemical Measurements. http://www.astm.org/Standards/G31. Retrieved 30 May 2016
12. Y. Choi, S. Nesic, S. Ling, Effect of H_2S on the CO_2 corrosion of carbon steel in acidic solutions. Electrochim. Acta **56**, 1752–1760 (2011)
13. ASTM NACE/ASTMG31 - 12a (2012) Standard Guide for Laboratory Immersion Corrosion Testing of Metals. http://www.astm.org/Standards/G31. Retrieved 05 May 2016
14. P. Venkatesan, B. Anand, P. Matheswaran, Influence of formazan derivatives on corrosion inhibition of mild steel in hydrochloric acid medium. Eur. J. Chem. **6**(S1), S438–S444 (2009)
15. W.B. Jensen, *The Lewis Acid-Base Concepts* (Wiley, New York, 1980), pp. 112–336
16. K. Fushimi, M. Seo, Initiation of a local breakdown of passive film on iron due to chloride ions generated by a liquid-phase ion-gun for local breakdown. J. Electrochem. Soc. **148**(11), B456–B459 (2001)
17. K. Fushimi, K. Azumi, M. Seo, Use of a liquid-phase ion-gun for local breakdown of the passive film on iron. J. Electrochem. Soc. **147**(2), 552–557 (2000)
18. K.E. Heusler, L. Fisher, Kinetics of pit initiation at passive iron. Mater. Corros. **27**(8), 551–556 (1976)
19. G.L. Song, Transpassivation of Fe-Cr-Ni stainless steels. Corros. Sci. **47**, 1953–1987 (2005)
20. J. Kruger, *Uhlig's Corrosion Handbook R. Winstone Revie (Ed.)* (Wiley, New Jersey, 2011)
21. M. Bojinov, G. Fabricius, T. Laitinen, T. Saario, Transpassivity mechanism of iron-chromium-molybdenum alloys studied by AC impedance, DC resistance and RRDE measurements. Electrochim. Acta **44**, 4331–4343 (1999)
22. A. Sara, Y. Yongsun, C. Pyungyeon, J. Changheui, B. Philip, Passivity breakdown of 316L stainless steel during potentiodynamic polarization in NaCl solution. Corros. Sci. **111**, 720–727 (2016)
23. G.S. Frankel, Pitting corrosion of metals: a review of the critical factors. J. Electrochem. Soc. **145**, 2186–2198 (1998)
24. H. Bohni, Breakdown of passivity and localized corrosion process. Langmuir **3**(6), 924–930 (1987)
25. R.T. Loto, Pitting corrosion evaluation of austenitic stainless steel type 304 in acid chloride media. J. Mater. Environ. Sci. **4**(4), 448–459 (2013)
26. H.H. Uhlig, Adsorbed and reaction-product films on metals. J. Electrochem. Soc. **97**, 215C–220C (1950)
27. R.T. Loto, Pitting corrosion evaluation and inhibition of stainless steels: a review. J. Mater. Environ. Sci. **6**(10), 2750–2762 (2015)
28. T.P. Hoar, D.C. Mears, G.P. Rothwell, The relationships between anodic passivity, brightening and pitting. Corros. Sci. **5**, 279–289 (1965)
29. G.S. Frankel, Pitting corrosion of metals: a review of the critical factors. J. Electrochem. Soc. **145**(6), 2186–2198 (1998)
30. N. Sato, A theory for breakdown of anodic oxide films on metals. Electrochim. Acta **16**, 1683–1692 (1971)
31. N. Sato, K. Kudo, T. Noda, The anodic oxide film on iron in neutral solution. Electrochim. Acta **16**, 1909–1921 (1971)
32. W. Fredriksson, S. Malmgren, T. Gustafsson, M. Gorgoi, K. Edström, Full depth profile of passive films on 316L stainless steel based on high resolution HAXPES in combination with ARXPS. Appl. Surf. Sci. **258**(15), 5790–5797 (2012)
33. K. Ahmad, *Principles of Corrosion Engineering and Corrosion Control* (Butterworth-Heinemann, Oxford, 2006)
34. J. Dong, J. Zhou, An investigation of pitting initiation mechanism of 1Cr12Ni2W1Mo1 V steel after induction hardening. J. Mater. Sci. **35**, 2653–2657 (2000)
35. H.H. Strehblow, P. Marcus, J. Oudar (eds.), *Corrosion Mechanisms in Theory and Practice* (Marcel Dekker, New York, 1995)
36. A. Bentour, S. Diamond, N.S. Berke, *Steel Corrosion in Concrete* (Chapman & Hall, London, 1997)
37. A.R. Brooks, C.R. Clayton, K. Doss, Y.C. Lu, On the role of Cr in the passivity of stainless steel. J. Electr. Sci. **133**, 2459–2464 (1986)